Lattice Boltzmann method based study of the heat transfer augmentation associated with Cu/water nanofluid in a channel with surface mounted blocks

Rasul Mohebbi [a,*], Hassan Lakzayi [a], Nor Azwadi Che Sidik [b,*], Wan Mohd Arif Aziz Japar [b]

[a] School of Engineering, Damghan University, Damghan 3671641167, Iran
[b] Malaysia – Japan International Institute of Technology (MJIIT), University Teknologi Malaysia Kuala Lumpur, Jalan Sultan Yahya Petra (Jalan Semarak), 54100 Kuala Lumpur, Malaysia

ABSTRACT

The study of the forced convection in a channel has many practical applications. In this paper, the forced convection heat transfer from surface mounted blocks attached to the bottom wall of a horizontal channel with nanofluid is numerically studied by the second-order lattice Boltzmann method (LBM). The effects of Reynolds numbers and geometrical parameters of the blocks in different aspect ratios on the flow field and temperature distribution for various volume fractions of nanofluid ($\varphi = 0$, 0.01, 0.03 and 0.05) are analyzed. Also, the influence of these parameters is investigated on the local and average Nusselt numbers. It is concluded that heat transfer in channels can be enhanced by using the block on the walls and adding nanoparticles. There is a maximum value of 39.04% increase in average heat transfer coefficient for all the examined cases compared to the base fluid (i.e., water).

© 2017 Elsevier Ltd. All rights reserved.

1. Introduction

Enhancement of forced convection heat transfer in a channel by using roughened surfaces such as rib, groove and obstacle in disturbing the fluid flow, and providing vortices is highly complex and a well-known method. It is an attractive research topic due to its wide range of applications in various fields of engineering, such as cross-flow heat exchanger, gas turbine airfoil cooling design, solar air heater blade cooling system, and gas cooled nuclear reactor [1–5].

The limited heat transfer capabilities of the conventional heat transfer liquids such as water, mineral oil and ethylene glycol demand innovative techniques to improve the heat transfer [6,7]. One way to enhance the heat transfer in separated regions is to employ nanofluids. The Argonne National Laboratory's research has been pioneering the use of particles nanometer dimensions. Nanofluids are fluids containing suspended nanoparticles with diameters below 100 nm [8]. Previous studies showed that a very small amount of nanoparticles exhibits enhanced thermal conductivity and convective heat transfer coefficients of inconsiderable

amplitude while the mixed fluid maintains stable suspensions [9–11].

Many numerical and experimental research studies have been conducted on the forced convection heat transfer in different geometry [12–14]. In addition to classic Navier–Stokes (NS), the particle-based methods, including direct simulation of Monte Carlo (DSMC), molecular dynamics (MD) and lattice Boltzmann method (LBM) are usually applied [15–17]. LBM has been proven to be an effective numerical tool for a large variety of complex fluid flows. The major benefits of using LBM are the simplicity of programming, locality of computation and natural parallelism [18–20].

A comparison study between the LBM and the finite element method (FEM) was presented for an incompressible, steady, laminar flow and heat transfer of power law fluid past a square cylinder by Mohebbi et al. [21]. It is obvious that the FEM and the LBM are two quite different numerical approaches. The FEM is based on approximations of flow equations that are governed by basic physical conservation laws at the macroscopic scale, whereas the LBM is based on evolution rules that obey the same conservation laws at the mesoscopic scale. In the LBM, the physical evolution rules are discrete; in the FEM, the discretization is performed at the level of the macroscopic flow equations. Thus, the LBM can be viewed as a minimal model for the Navier–Stokes equations instead of a full molecular dynamics approach. Indeed, the fluid flow is mainly determined by the collective behavior of many molecules not by

---

the detailed molecular interactions. As the Boltzmann equation is kinetic-based, the physics associated with the molecular level interaction can be incorporated more easily in the LBM. They showed that the LBM consumes less memory (about 1/18 times less than the FEM does) and it also requires a shorter computational time in comparison to the FEM. Moreover, it has appeared that the FEM faces more difficulties in predicting the complex geometry. With the FEM, a not-fine-enough mesh will most probably lead to a poor estimate of the flow field and heat transfer.

Several studies were conducted on the forced convection fluid flow and heat transfer by utilizing extended surfaces in a channel, but there were only a few studies solving the nanofluid forced convection in a ribbed channel. Young and Vafai [22] studied the effects of controlling parameters on cooling the heated channels with mounted objects. Their focus was to test the effects of changing the dimensions of the object, the thermal conductivity, the heating method, and the Reynolds number. They found the narrow gaps between tall obstacles allowing the upstream thermal transport by the cavity vortices through the reduced cavity-core flow interaction. Also, differences between surface flux and volumetric heating manifest themselves in the isotherms within the obstacles with only small changes in Nusselt numbers. The researchers concluded that the fluid flow and heat transfer were affected by the geometry and the material of the object. Chandra et al. [23] investigated the heat transfer of a fully developed turbulent flow in a channel with heated ribs mounted on the one, two, three and four channel sides. They concluded that the heat transfer and the friction factor were enhanced by increasing the number of walls containing ribs.

A numerical study for a laminar flow and heat transfer in a three-dimensional channel with staggered rows of rectangular blocks was conducted by Nakajima et al. [24]. The heat transfer coefficient of the blocks faces was found to change from one face to another which was also affected by altering the Reynolds number. They found that the mean Nusselt number would insignificantly vary on the side surfaces of the blocks as the Reynolds number changed. In addition, the mean Nusselt number decreased as the flow was passing over more block rows, yet most of the flow and heat transfer characteristics started to change around the third-row block. Lu and Jiang [25] investigated the forced convection heat transfer in a rectangular channel with ribs of different rotated angles. Their numerical results indicated that the heat transfer coefficients were the largest with the 60 degree ribs, but the channel with the 20 degree ribs had the best overall thermal/hydraulic performance considering the heat transfer and the pressure drop when the spacing between ribs was 4 mm.

Yang and Chen [26] carried out a numerical simulation to investigate the influence of transient flow field structures, and the heat transfer characteristics of heated blocks in the channel with a transversely oscillating cylinder. Moussaoui et al. [27] applied the multi-relaxation time lattice Boltzmann equation for the numerical prediction of a laminar and convective heat transfer through a 2D obstructed channel flow. Similarly, the forced convection heat transfer using the LBM in a channel with extended surfaces was studied by Alamyane and Mohamad [28]. They concluded that the closer the objects the better the heat transfer would become and as the height of the objects increased, the temperature in spacing increased. Also, they showed for the ratio of the object's height to the channel's height more than 0.5, any extra length of the object did not contribute to the rate of heat transfer.

Pirouz et al. [29] studied a numerical simulation of conjugate heat transfer in a rectangular channel with wall-mounted obstacles. They reported that reducing the distance between obstacles would make the flow deviate and accelerate in the vicinity of faces and would cause an increase in the rate of convective heat transfer from the obstacles. Also, they found the thermal diffusivity of the

obstacle to play an important role in the conjugate heat transfer rate through the obstacle. Due to the reduction of the internal resistance to heat flow, the higher quantities of energy were removed from the obstacle faces, as thermal diffusivity increased.

Sidik et al. [30] presented a numerical study on the thermal performance of fins mounted on the bottom wall of a horizontal channel using the LBM. They examined the heat transfer performance by adding the fin and using the nanofluid. Their result showed that the heat transfer rate of fins was significantly affected by the Reynolds number and the thermal conductivity of the fins.

In general, the previous literature investigated different cases of fluid flow and heat transfer in channels with mounted objects while further research is recommended to study the forced heat transfer in a channel with nanofluid, while rectangular blocks connected to the bottom wall. In this study, we used the LBM for simulating the forced convection fluid flow and heat transfer of Cu/water nanofluids over a series of extended surfaces mounted in the bottom wall of a channel. To the best of authors' knowledge, this is the first time the LBM was used on the combination of the different geometrical parameters of the blocks and nanofluid in a channel. Beside investigating the effect of different aspect ratio of mounted blocks, the objective of the present paper was to investigate the effect of various solid volume fractions of Cu/water nanofluid on heat transfer performance in straight channel.

2. Geometry of the problem

In this study, we investigated the forced convection heat transfer of the nanofluid between two parallel plates with a staggered arrangement of blocks attached to the bottom walls which are shown in Fig. 1.

The channel and blocks were heated and kept at a constant temperature T_w. A cold mixture of base fluid (water) and the nanoparticles (Cu) by constant temperature T_{in} and uniform velocity u_{in}, was forced to flow into the channel. To minimize the influence of the outflow boundary condition, a sufficient channel length was selected with the ratio of channel length to height L/H = 25. The height and width of blocks were denoted with h and w, respectively, whereas the extended surfaces' height to the height of the channel with the ratio B = h/H were 0.1, 0.3 and 0.5. The ratio between the objects' distance of the channel's height A = l/H was fixed at 1.0.

The inflow blocks were located at an upstream distance x/L = 0.2. Reynolds numbers were 10, 40, and 70. The flow was assumed as Newtonian, laminar, two-dimensional, and incompressible. In addition, it was assumed that the cold mixture of base fluid (water) and the solid spherical nanoparticles (Cu) was in thermal equilibrium and it would flow at the same velocity as a homogenous mixture. Thermophysical properties of the nanoparticles and the base liquid are gathered in Table 1.

3. Numerical simulation

3.1. Lattice Boltzmann method

3.1.1. Lattice Boltzmann equation of velocity field

The D2Q9 LBM model was used to simulate fluid flow in a two-dimensional channel with the uniform grid size of δx by δy. The lattice Boltzmann equation (known as LBGK equation) with single relaxation time can be expressed as [14,32,33]:

$$f_i(x + e_i \delta t, t + \delta t) - f_i(x,t) = -\frac{1}{\tau_v}[f_i(x,t) - f_i^{eq}(x,t)] \qquad (1)$$

where $f_i(x,t)$ is a distribution function in space x and time t; $f_i^{eq}(x,t)$ is the equilibrium distribution function, x denotes the discrete
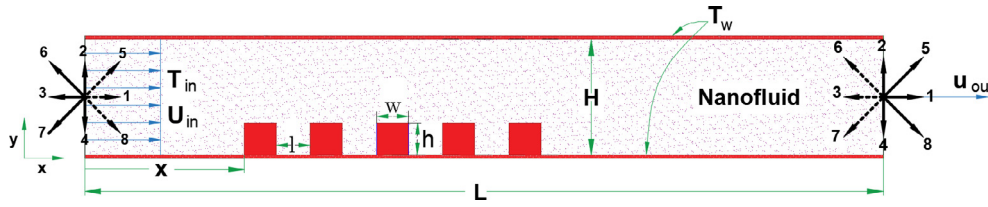
Fig. 1. Schematic diagram of physical system.

Table 1
Thermo-physical properties of the base fluid and the nanoparticles [31].

Property	Fluid phase (Water)	CuO(nanoparticles)
C_p (J/kg K)	4179	383
ρ (kg/m^3)	997.1	8954
k (W/m K)	0.613	400
$\beta \times 10^5$ (K^{-1})	21	1.67
$\mu \times 10^4$ (kg/ms)	8.55	

velocity set, τ_v is the dimensionless relaxation of the velocity field, and δt is the time step. In Eq. (1), the equilibrium distribution function is as follows [34–36]:

$$f_i^{eq} = w_i \rho \left[1 + 3 \frac{e_i \cdot u}{c^2} + \frac{9}{2} \frac{(e_i \cdot u)^2}{c^4} - \frac{3}{2} \frac{u^2}{c^2} \right] \qquad (2)$$

where w_i is the weighting coefficient and $c = \delta x / \delta t$ in this model:

$$e_i = \begin{cases} (0,0) & (i = 0) \\ (\cos[(i-1)\pi/2], \sin[(i-1)\pi/2]) \cdot c & (i = 1, \ldots, 4) \\ \sqrt{2}(\cos[(i-5)\pi/2 + \pi/4], \sin[(i-5)\pi/2 + \pi/4]) \cdot c & (i = 5, \ldots, 8) \end{cases} \qquad (3)$$

$$w_i = \begin{cases} \frac{4}{9} & (i = 0) \\ \frac{1}{9} & (i = 1, \ldots, 4) \\ \frac{1}{36} & (i = 5, \ldots, 8) \end{cases} \qquad (4)$$

The relaxation time for the flow field, τ_v can be defined as

$$\tau_v = 0.5 + v \frac{\delta t}{c_s^2} \qquad (5)$$

where v is kinematic viscosity and $c_s = c/\sqrt{3}$ is the speed of sound and v is calculated by Reynolds number as

$$v = \frac{u_{in} \cdot 2H}{Re} \qquad (6)$$

The macroscopic velocity and macroscopic density can be evaluated as

$$\rho = \sum_{i=0}^{8} f_i \qquad (7)$$

$$\rho u = \sum_{0}^{8} f_i e_i \qquad (8)$$

3.1.2. Lattice Boltzmann equation of temperature field

Prediction of thermal field requires a new type of distribution function to represent the evolution of internal energy [37–39]. The most common type of internal energy distribution function is the nine-velocity model. The governing equation is expressed as

$$g_i(x + e_i \delta t, t + \delta t) - g_i(x, t) = -\frac{1}{\tau_g} [g_i(x, t) - g_i^{eq}(x, t)] \qquad (9)$$

The equilibrium distribution function is expressed as

$$g_i^{eq} = w_i T \left[1 + 3 \frac{e_i \cdot u}{c^2} \right] \qquad (10)$$

Here, τ_g is a single relaxation collision frequency for temperature distribution function and it can be defined as

$$\tau_g = 3\alpha + 0.5 \qquad (11)$$

where α can be calculated by the value of a fixed parameter $Pr = v/\alpha$. The value of the macroscopic fluid temperature can be evaluated from [40]

$$T = \sum_{i=0}^{8} g_i \quad (i = 0, 1, \ldots, 8) \qquad (12)$$

3.2. Nanofluid

The thermophysical properties of nanofluid are mostly the functions of particle volumetric concentration. In the absence of experimental data, nanofluid density and specific heat are defined only as a function of volume fraction as follow [41–44]

$$\rho_{nf} = (1 - \varphi)\rho_f + \varphi \rho_p \qquad (13)$$

$$(\rho c_p)_{nf} = (1 - \varphi)(\rho c_p)_f + \varphi(\rho c_p)_p \qquad (14)$$

In the equations above, subscripts "f", "p" and "nf" refer to base fluid, nanoparticle and the nanofluid, respectively. The nanofluid thermal diffusivity can be obtained by [45]:

$$\alpha_{nf} = \frac{k_{nf}}{(\rho c_p)_{nf}} \qquad (15)$$

Even though many models have been developed to predict the nanofluid viscosity and thermal conductivity [46], the most common models used in the literature are the Brinkman [47] model and Patel et al. [48] model, which are

$$\mu_{nf} = \mu_f / (1 - \phi)^{2.5} \qquad (16)$$

$$\frac{k_{nf} - k_f}{k_f} = \frac{k_p}{k_f} \left(1 + c \frac{u_p d_p}{\alpha_f} \right) \frac{d_f}{d_p} \frac{\varphi_p}{1 - \varphi_p} \qquad (17)$$

where c is a constant and equal to 25,000 for a wide range of experimental data [48] and u_p is the Brownian velocity for nanoparticles and can be determined as:

$$u_p = \frac{2 k_B \theta}{\pi \mu_l d_p^2} \qquad (18)$$

in which k_B is the Boltzmann constant and θ is the temperature in Kelvin. The following equation can be used to compute the nanofluid Prandtl number:

$$Pr_{nf} = \frac{(\mu c_p)_{nf}}{k_{nf}} \qquad (19)$$

3.3. Boundary conditions

Computational codes can produce reliable and accurate results if proper boundary conditions can be implemented. Boundary conditions play a crucial role in the stability and accuracy of numerical scheme [49]. In LBM-based numerical simulations, it seems necessary to transform density, velocity, and temperature boundary conditions which conform at mesoscale levels for a distribution function [50]. Regarding the boundary conditions of the flow field, the solid walls are assumed to be no slip, thus the bounce-back scheme is applied [51–53] in which the distribution functions pointing to the fluid are equal to those pointing out of the domain.

Since the inlet velocity of the flow is specified, the inward distribution functions should be computed at the boundary. So, the values of the distribution functions f_1, f_5, f_8 at the inlet (see Fig. 1) along with the density ρ are the unknowns; however, f_3, f_6 and f_7 are known from the streaming step. In the current study, the Zou–He model [52] was used at the inlet of the computational domain in the LBM. The four equations are solved, and the desired unknown distribution functions are calculated as follows:

$$\rho_{in} = \frac{[f_0 + f_2 + f_4 + 2(f_3 + f_6 + f_7)]}{(1 - u_{x\,in})} \qquad (20)$$

$$f_1 = f_3 + \frac{2}{3}\rho_{in}u_{xin} \qquad (21)$$

$$f_5 = f_7 + \frac{1}{6}\rho_{in}u_{xin} + \frac{1}{2}\rho_{in}u_{yin} - \frac{1}{2}(f_2 - f_4) \qquad (22)$$

$$f_8 = f_6 + \frac{1}{6}\rho_{in}u_{xin} + \frac{1}{2}\rho_{in}u_{yin} + \frac{1}{2}(f_2 - f_4) \qquad (23)$$

An extrapolation scheme, as proposed by Mei et al. [54], was used to simulate the outlet flow condition in the LBM. Here the unknowns for outlet are f_3, f_6, and f_7 as these are coming from outside the computational domain (see Fig. 1) which theirs values are obtained by following:

$$f_3^n = 2f_3^{n-1} - f_3^{n-2} \qquad (24)$$

$$f_6^n = 2f_6^{n-1} - f_6^{n-2} \qquad (25)$$

$$f_7^n = 2f_7^{n-1} - f_7^{n-2} \qquad (26)$$

The constant temperature in the thermal boundary condition was adopted for the inlet, top and bottom walls of flow field and walls of the blocks. The inlet fluid was set to the value of zero, $T_{in} = 0$, and the solid walls had the constant value temperature, $T_w = 1$. Here, the introduced method by Mohamad [55] was employed to treat the constant temperature boundary conditions and the outlet boundary by solving the values of the unknown thermal distribution functions coming into the computational domain from outside the domain. For instance, the constant temperature boundary for inlet is applied using:

$$g_1 = T_{in}(w_1 + w_3) - g_3 \qquad (27)$$

$$g_5 = T_{in}(w_5 + w_7) - g_7 \qquad (28)$$

$$g_8 = T_{in}(w_8 + w_6) - g_6 \qquad (29)$$

For channel outlet, a second order extrapolation are as follows:

$$g_3^n = 2g_3^{n-1} - g_3^{n-2} \qquad (30)$$

$$g_6^n = 2g_6^{n-1} - g_6^{n-2} \qquad (31)$$

$$g_7^n = 2g_7^{n-1} - g_7^{n-2} \qquad (32)$$

3.4. Results and discussion

3.4.1. Grid independency and validation

Having studied the grid independency for the code, as shown in Table 2, a lattice with 101 × 2501 nodes was found appropriate for the next computations considering the computational cost and numerical accuracy. The local Nusselt number calculated in the bottom wall was defined by Eq. (33) [13],

Table 2
Effect of the mesh size on average Nusselt number for Re = 10, ϕ = 0.05 and B = 0.5.

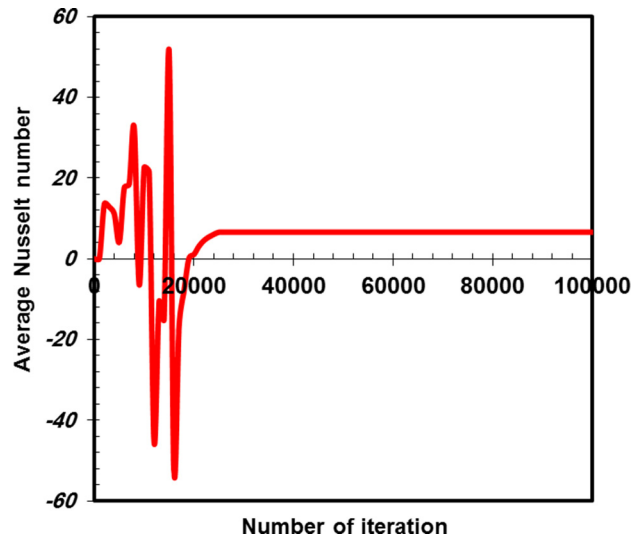| Number of nodes	Average Nusselt number
51 × 1251	7.6583
101 × 2501	6.5579
201 × 5001	6.5425

Fig. 2. Variation of average Nusselt number versus number of iterations for Re = 10, ϕ = 0.05 and B = 0.5.
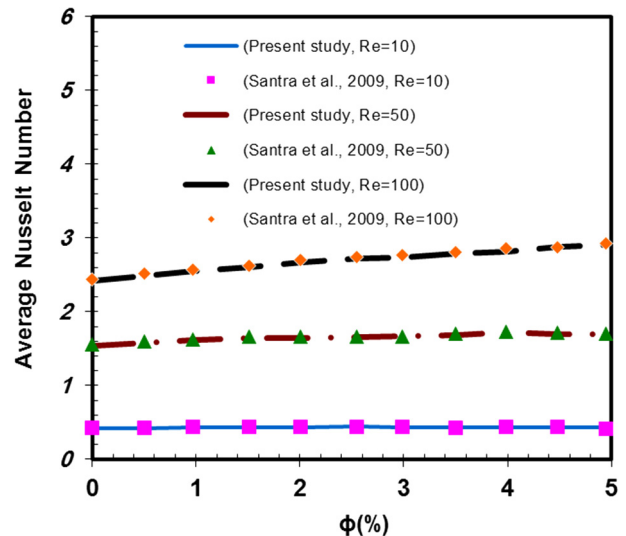

Fig. 3. Comparison of the average Nusselt number at different solid volume fractions of nanofluid to Santra et al. [56].
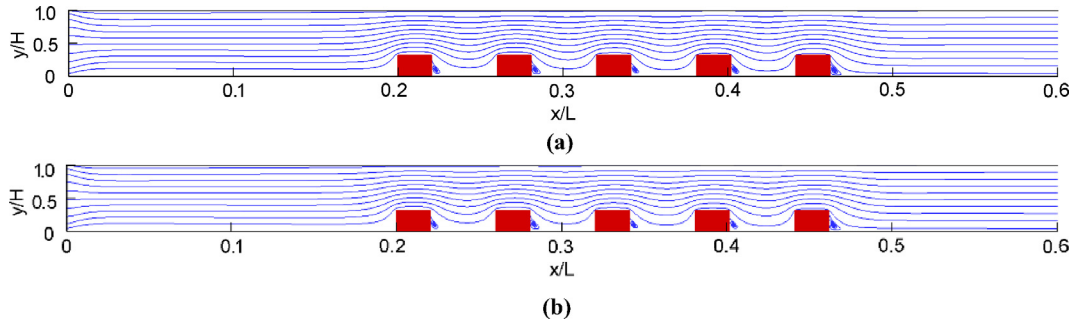
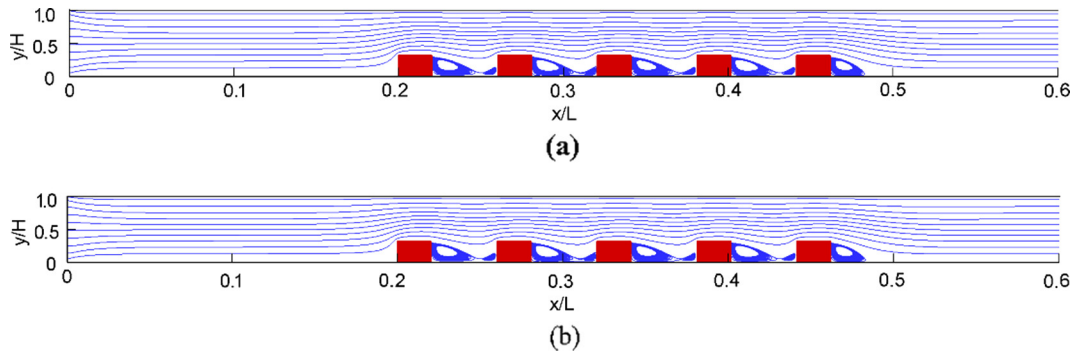**Fig. 4.** Variations of the streamlines in the channel versus ϕ at Re = 10 for B = 0.3, (a) ϕ = 0.0, (b) 0.05.

Fig. 5. Variations of the streamlines in the channel versus ϕ at R = 70 for B = 0.3, (a) ϕ = 0.0, (b) 0.05.

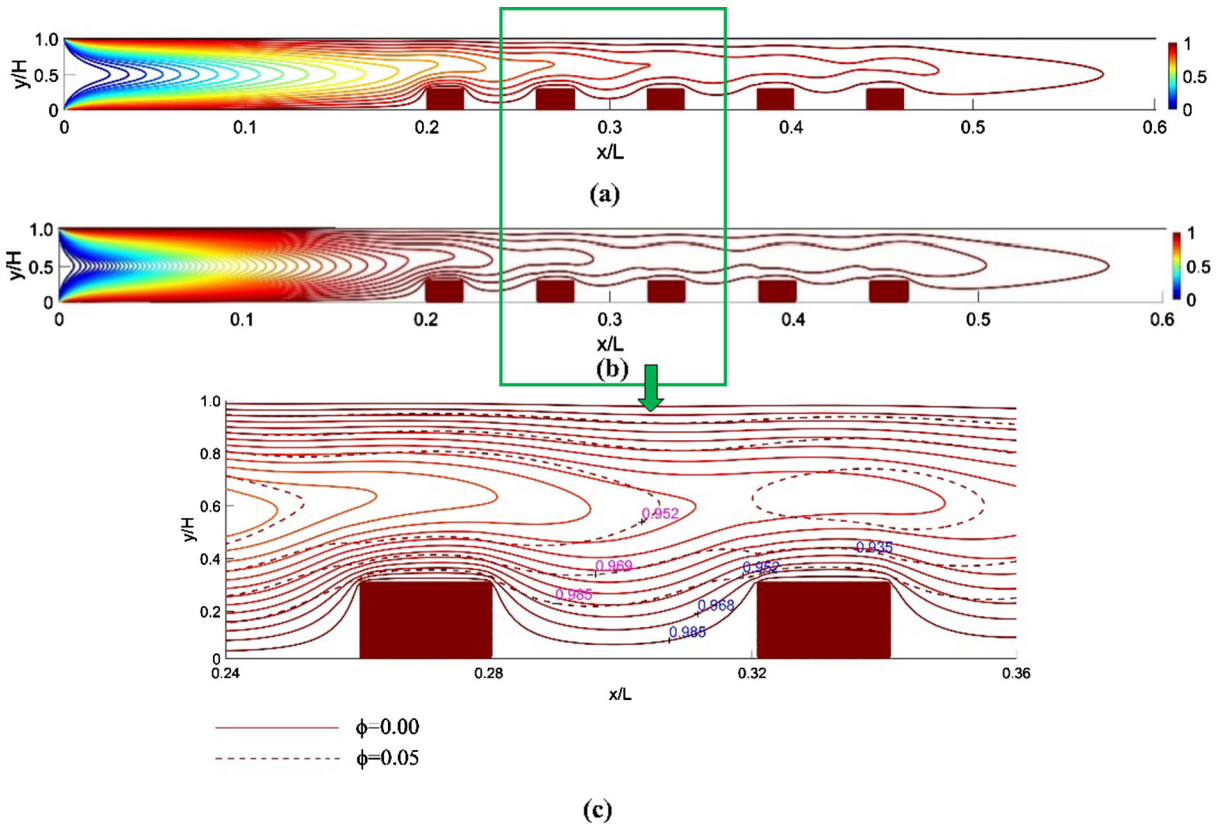**Fig. 6.** Variations of the isotherms in the channel versus ϕ at Re = 10 for B = 0.3, (a) ϕ = 0.0, (b) 0.05, (c) Comparisons of dimensionless isotherm contours for the pure fluid (ϕ = 0.0) and nanofluid (ϕ = 0.05).

Fig. 7. Variations of the isotherms in the channel versus ϕ at $Re = 70$ for B = 0.3, (a) $\phi = 0.0$, (b) 0.05, (c) Comparisons of dimensionless isotherm contours for the pure fluid ($\phi = 0.0$) and nanofluid ($\phi = 0.05$).
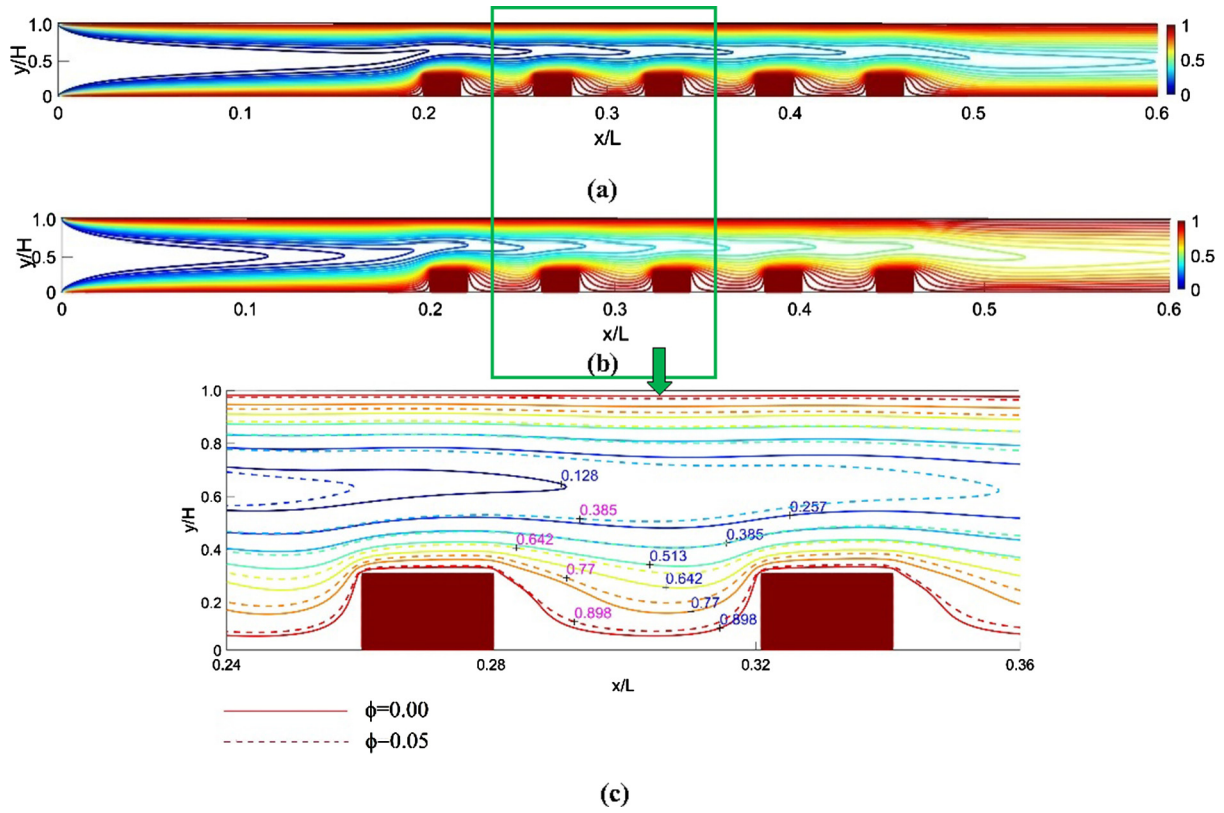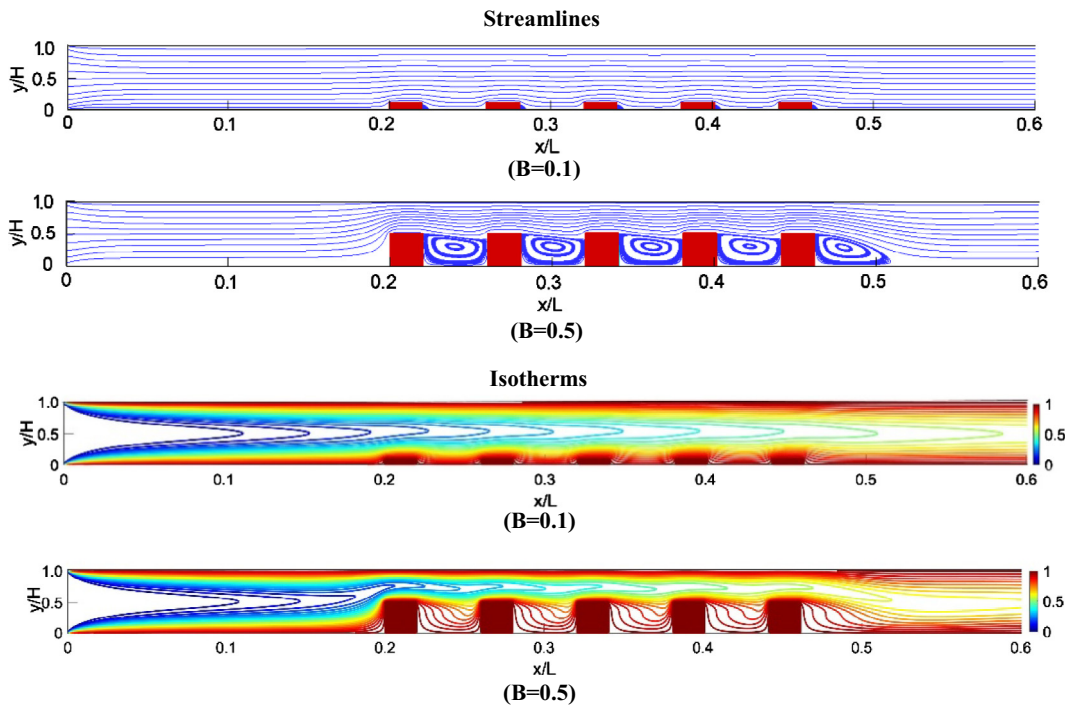

Fig. 8. Streamlines and isotherm contours for $Re = 70$ and $\phi = 0.05$.
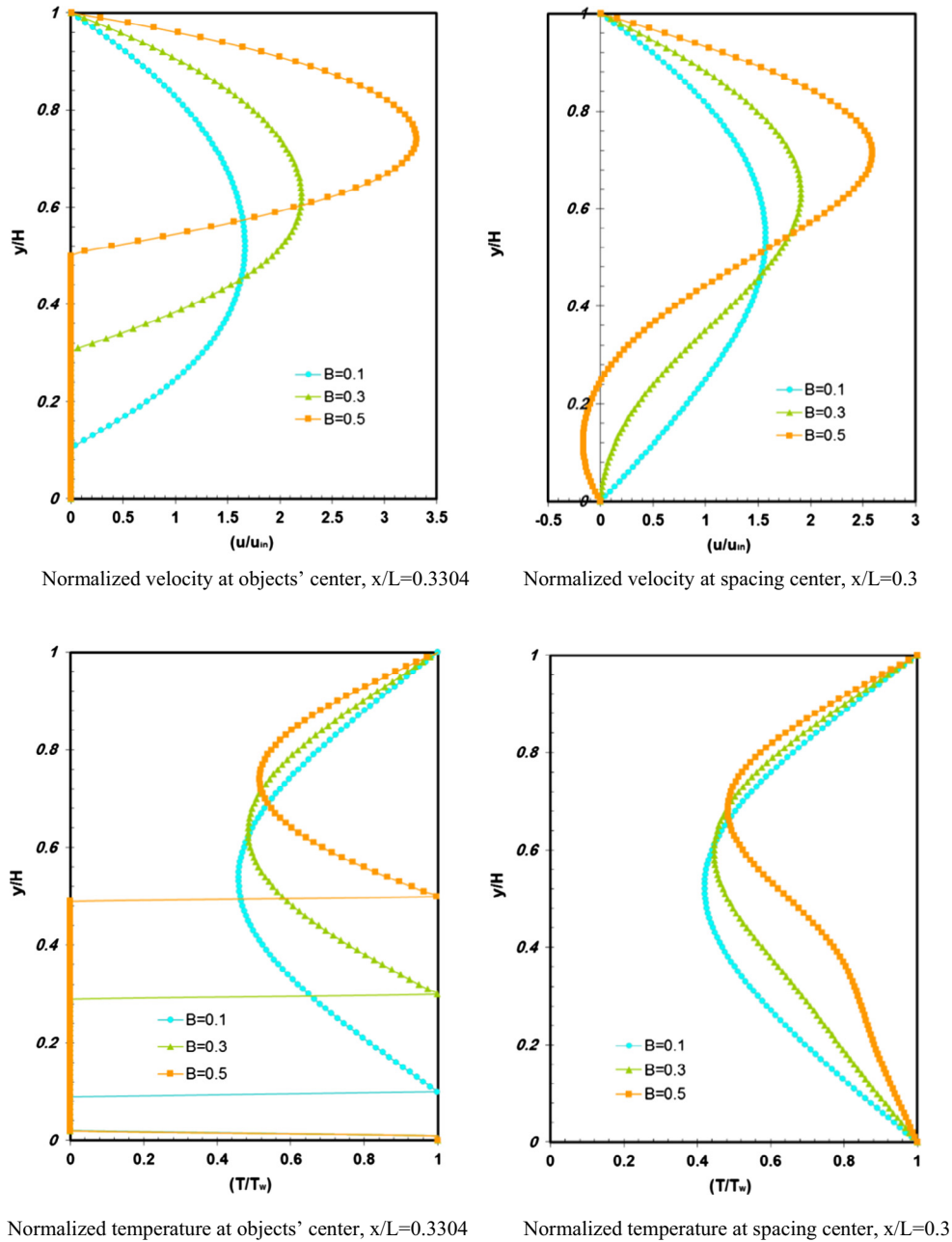
Normalized velocity at objects' center, x/L=0.3304

Normalized velocity at spacing center, x/L=0.3

Normalized temperature at objects' center, x/L=0.3304

Normalized temperature at spacing center, x/L=0.3

Fig. 9. Velocity and temperature profiles of various block's aspect ratio for $Re = 40$, $\varphi = 0.03$.

$$Nu = -\frac{2H \cdot \frac{\partial T}{\partial y}\big|_{y=0}}{T_w - T_b} \qquad (33)$$

where T_b defined as,

$$T_b = \frac{\int_0^H u \cdot T dy}{\int_0^H u dy} \qquad (34)$$

To obtain a correct convergence of the numerical simulation, the averaged Nusselt number was plotted against the number of iterations, for $Re = 10$, $\phi = 0.05$ and B = 0.5. The computation was continued to achieve a constant trend (as shown in Fig. 2). In other words, the results were assumed to converge when the average Nusselt number would approach a constant value. In order to assess the accuracy of the undertaken numerical procedure, the algorithm for the 2D channel with the length to height ratio, L/H = 100 at different Reynolds numbers was examined. The variation

of the average Nusselt number of the present computations along the hot wall was compared to those in Santra et al. [2009] at Re = 10, 50 and 100 and to the different solid volume fraction of the nanofluid. The comparisons are presented in Fig. 3. They are in acceptable accuracy relative to those in the literature.

4. Results and discussion

The present computations have been carried out for Re = 10, 40 and 70, five block numbers by different block ratios B = 0.1, 0.3 and 0.5, A = 1.0, and volume fractions of nanofluid ϕ = 0–0.05. The effect of volume fractions of the nanofluid on streamlines and isotherms inside the channel are shown in Figs. 4–7 for different Reynolds numbers at B = 0.3. As the flow was approaching the blocks, the streamlines were deflected toward the top wall. Therefore, in the region near the blocks, the streamlines were more densely

packed. A weak circulation eddy was formed behind the blocks in low Re. The strength and length of the vortices behind every block would increase with increasing the Reynolds number which caused an increase in the magnitude of the vortices due to a high flow velocity. There was no significant effect on the streamlines by changing the volume fractions of nanofluid.

Figs. 6 and 7 demonstrate isotherms. The enlarged isotherms clearly show the isotherm lines behavior near the channel walls. As shown in these figures, because of the higher thermal conductivity of the nanofluid, the nanofluid temperature was higher than the pure water in every point in the channel. In other words, in each Reynolds number, the thermal boundary layer was thickened with ϕ, i.e.$\delta_{t,nf}/\delta_{t,f} > 1$. This phenomena can be explained based on the analytical solution for a simplified case of external flow over a flat plate as shown in $\delta_t \cong \delta/Pr^{1/3}$ [57], where δ is the hydrodynamic boundary layer ($\delta = 5x/Re_x^{0.5}$; with x being the distance from the plate leading edge).

Using the values of ρ_{nf} and μ_{nf} (from Eqs. (14) and (16), it can be shown that $\delta_{t,f}/\delta_{t,nf} = (\nu_f/\nu_{nf})^{0.5}.(Pr_{nf}/Pr_f)^{1/3}$;where $\nu = \mu/\rho$. The ratios (ν_f/ν_{nf}) and (Pr_{nf}/Pr_f) can be expressed in terms of ϕ. The variation of the terms (ν_f/ν_{nf}), (Pr_{nf}/Pr_f) and $\delta_{t,f}/\delta_{t,nf}$ with ϕ has been shown in three separate curves in [58] in full detail where $\delta_{t,nf}/\delta_{t,f} > 1$. It demonstrates that the thermal boundary layer thickness increases with ϕ. Also, it can be shown from these figures that by increasing the Reynolds number, the thermal boundary layer was condensed toward the walls, which eventually lead to the increasing temperature gradient near the wall and enhanced heat transfer. In other words, at low Reynolds numbers, the conduction was the dominating mechanism of heat transfer, therefore, the isotherms stretched above the blocks and took a larger area in the channel. As Re increased, the convection became the dominating mechanism, and the strong cold inlet flow pushed the isotherms near the bottom walls.

Fig. 8 shows the streamlines and the isotherm contours for *Re* = 70, ϕ = 0.05 and for B = 0.1 and 0.5. Similar to the case of B = 0.3, the effect of blocks on the flow pattern and the structure of the vortexes were clearly observed. Simulations showed that the vortex behind the blocks became larger and covered more area as the aspect ratio B increased, due to increasing resistance to the flow. Also, the temperature values were affected by the increase of the block's aspect ratio B where heat was circulating at higher ratio B. It seemed that the right faces of the blocks by B = 0.5 became hotter than the left faces due to the formation of the bigger clockwise vortices which carried heat from left faces to the right ones of the previous block.

The velocity and temperature distributions in the channel for various blocks aspect ratio at *Re* = 40 and φ = 0.03 are shown in Fig. 9. The highest value of the velocity distribution was obtained for B = 0.5. The negative values emerged due to the circulation of the flow behind the objects. Also, the temperature variation indicated that the highest values at the center of spacing were obtained at higher blocks aspect ratio.

Variation of the local Nusselt number for different values of nanofluid 0, 0.01, 0.03 and 0.05 in *Re* = 40 and B = 0.3 is plotted in Fig. 10. This figure demonstrates that the local Nusselt number increases with the increasing volume fraction of nanofluid, due to the increase of the thermal conductivity of the nanofluid. This indicates the merit of employing the nanofluid for enhanced heat transfer. Also, the emergence of a large value of the local Nusselt number near the corners of the blocks due to the large temperature gradient normal to the surface of the blocks leads to the high value of the convective heat transfer coefficient as a considerable effect. The rise in Nusselt number in the wake of blocks was due to the vortex formation. However, far from the blocks, the local Nusselt number decreases to a fixed value.
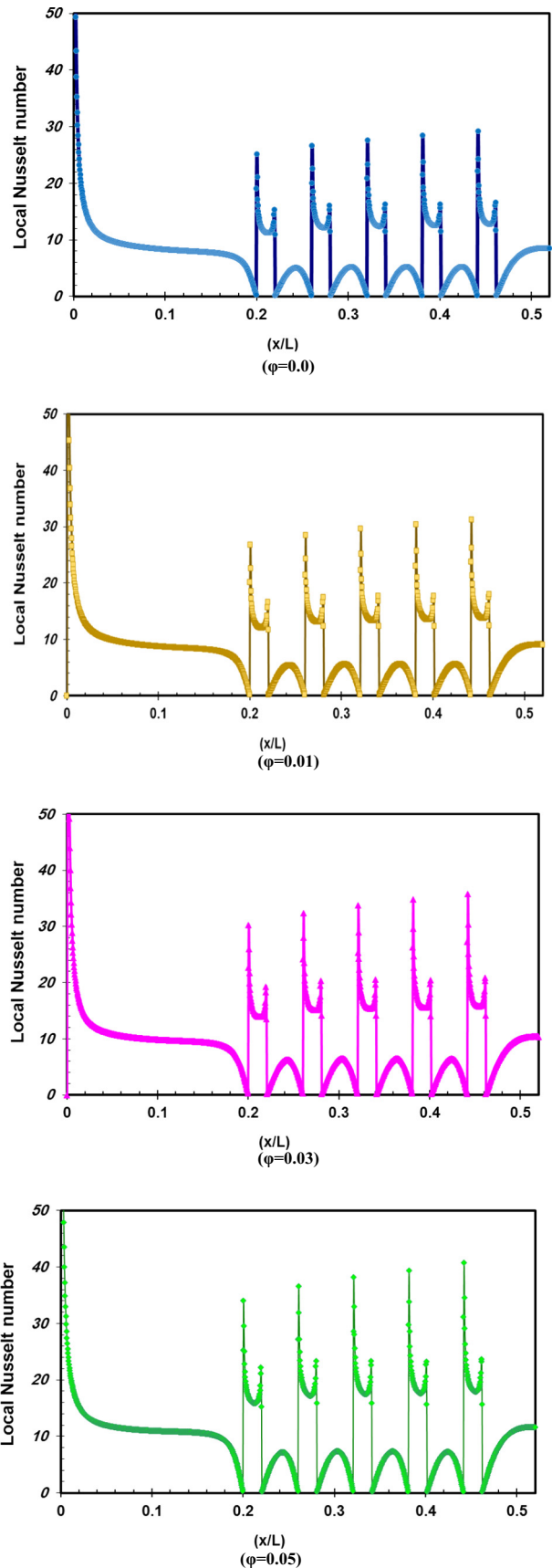

Fig. 10. Local Nusselt number in different volume fraction of nanofluid for *Re* = 40, B = 0.3.

Fig. 11 shows the variations of local Nusselt number along the channel wall for different blocks aspect ratio B at $Re = 40$ and ϕ
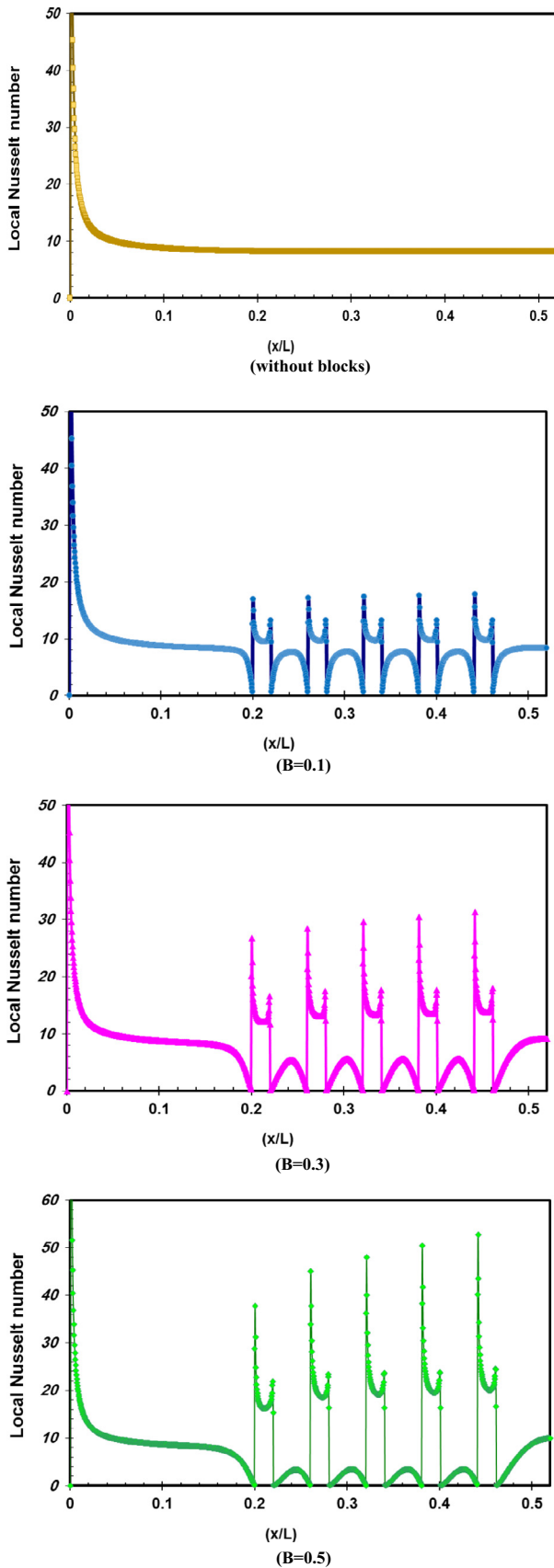

Fig. 11. Local Nusselt number in different block aspect ratio B for $Re = 40$, $\varphi = 0.01$.

= 0.01. A similar trend, according the Fig. 10, is observed by analysis of the different aspect ratio of blocks. It is observed that the local Nusselt number and the heat transfer rate increase with the increase of aspect ratio B. The maximum value of Nusselt number is found to be 52.7241 occurred at the corner of the last block by B = 0.5. Also, it is clear that inserting the blocks in channel wall would lead to increasing the heat transfer rate in the related section.

The average Nusselt number (from x/L = 0.04–0.56) was calculated for all volume fractions of nanofluid and all values of aspect ratio at different Reynolds numbers. The effect of φ and Re on the rate of heat transfer for B = 0.3 is shown in Fig. 12. Accordingly, as the Re increases at a fixed solid volume fraction of nanofluid, the average Nusselt number reaches high values which means the enhancement of heat transfer occurs at high Re. By increasing the volume concentration, the average Nusselt number increases linearly and has the highest value for the $\phi = 0.05$. This effect was caused as the rate of heat transfer for the water-based nanofluid with Cu nanoparticles was found to be more effective than the base fluid due to a higher thermal conductivity of solid nanoparticles than the pure fluids. By increasing the nanoparticle volume fraction from 0 to 0.05, the heat transfer rates for Re = 10, 40 and 70 increased to 29.20%, 39.04% and 35.12%, respectively. Also the higher value of averaged Nu equal to 10.6618 was obtained at $\varphi = 0.05$ and Re = 70.

Fig. 13 shows the variation of average Nu number at a different solid volume fraction of nanofluid and various aspect ratio B at Re
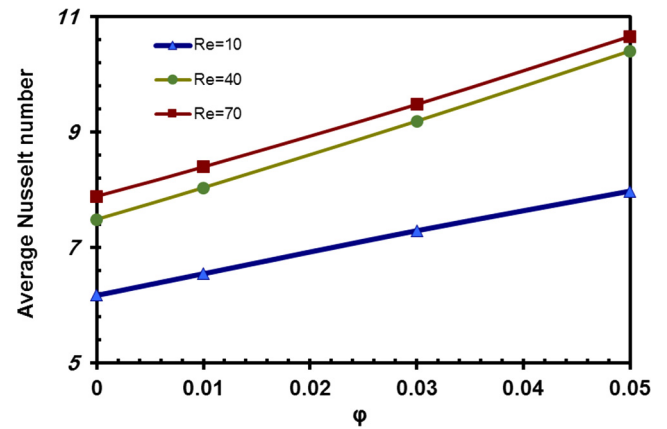

Fig. 12. The averaged Nusselt number for a different solid volume fraction of nanofluid and various Reynolds numbers at B = 0.3.
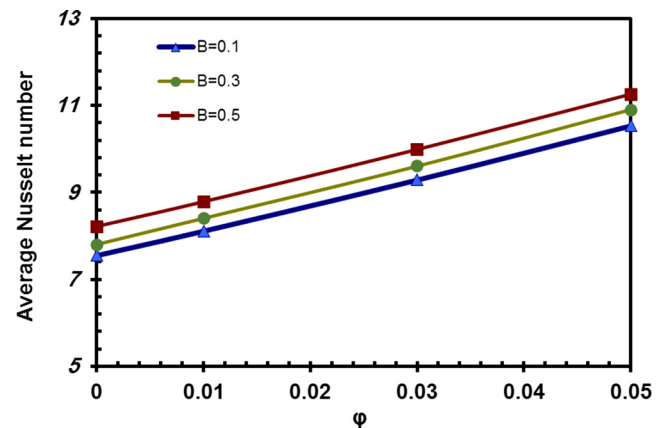

Fig. 13. The averaged Nusselt number for a different solid volume fraction of nanofluid and various aspect ratio B at $Re = 40$.

= 40. It can be seen that there was an increasing behavior in the heat transfer rate with increasing the aspect ratio. This implies that heat transfer improvement resulting from the water–Cu nanofluids addition was improved when the block aspect ratio was higher. Also, as shown in these figures, the average Nu number increased with φ as the thermal conductivity of the nanofluid increased with φ according to Eq. (17).

5. Conclusion

Two-dimensional numerical simulations using the LBM were carried out to understand the effect of nanofluid on the forced convective flow and heat transfer in a channel with surface mounted blocks. The main focus of the present paper was to investigate the effects of Reynolds number, blocks aspect ratio and solid volume fraction of nanofluid on the flow field, temperature distribution, local and average Nusselt number. The combination of different geometrical parameters of the blocks and using nanofluid in a channel are innovative in the present study. It was observed that the construction of the blocks at the bottom wall by formation of vortices and addition of nanoparticles to the pure fluid could significantly enhance the heat transfer. Local Nusselt number distribution along the lower wall was reported as its variation with nanofluid volume fraction and blocks aspect ratio demonstrated that heat transfer was improved with increasing φ and B. The study of average Nusselt number was carried out where a substantial increase in the average Nu was reported. The maximum value of Nusselt number is found to be 52.7241 occurred at the corner of the last block by B = 0.5. Interpreting the simulation results, the increase in the Reynolds number increases, the rate of heat transfer, too. Also, the higher value of averaged Nu equal to 10.6618 was obtained at φ = 0.05 and *Re* = 70.

Conflict of interest

The authors declare that there is no conflict of interest.

References

[1] E. Kianpour, I. Golshokouh, The effects of row trench holes with alignment angle of +60 degrees on film cooling effectiveness at low blowing ratios, J. Adv. Res. Fluid Mech. Therm. Sci. 4 (2014) 24–35.
[2] S. Salimi, A. Fazeli, E. Kianpour, Film cooling effectiveness using cylindrical and compound cooling holes at the end wall of combustor simulator, J. Adv. Res. Fluid Mech. Therm. Sci. 1 (2014) 38–43.
[3] A.N. Al-Shamani, K. Sopian, H. Mohammed, S. Mat, M.H. Ruslan, A.M. Abed, Enhancement heat transfer characteristics in the channel with Trapezoidal rib–groove using nanofluids, Case Stud. Therm. Eng. 5 (2015) 48–58.
[4] I.A. Ghani, N.A.C. Sidik, R. Mamat, G. Najafi, T.L. Ken, Y. Asako, et al., Heat transfer enhancement in microchannel heat sink using hybrid technique of ribs and secondary channels, Int. J. Heat Mass Transf. 114 (2017) 640–655.
[5] D. Jehad, G. Hashim, Numerical prediction of forced convective heat transfer and friction factor of turbulent nanofluid flow through straight channels, J. Adv. Res. Fluid Mech. Therm. Sci. 8 (2015) 1–10.
[6] N.A.C. Sidik, M.N.A.W. Muhamad, W.M.A.A. Japar, Z.A. Rasid, An overview of passive techniques for heat transfer augmentation in microchannel heat sink, Int. Commun. Heat Mass Transf. 88 (2017) 74–83.
[7] R. Gugulothu, K.V.K. Reddy, N.S. Somanchi, E.L. Adithya, A review on enhancement of heat transfer techniques, Mater. Today: Proc. 4 (2017) 1051–1056.
[8] S.U.S. Choi, Enhancing thermal conductivity of fluids with nanoparticles. American Society of Mechanical Engineers, Fluids Engineering Division (Publication) FED, 1995, pp. 99–105.
[9] G. Li, M. Aktas, Y. Bayazitoglu, A review on the discrete Boltzmann model for nanofluid heat transfer in enclosures and channels, Num. Heat Transf. Part B: Fundam. 67 (2015) 463–488.
[10] N.A.C.S. Darminesh Sathuramalingam Pillay, Tribological properties of biodegradable nano-lubricant, J. Adv. Res. Fluid Mech. Therm. Sci. 33 (2017) 1–13.
[11] M.H. Hamzah, N.A.C. Sidik, T.L. Ken, R. Mamat, G. Najafi, Factors affecting the performance of hybrid nanofluids: a comprehensive review, Int. J. Heat Mass Transf. 115 (2017) 630–646.
[12] M. Nazari, M. Kayhani, R. Mohebbi, Heat transfer enhancement in a channel partially filled with a porous block: lattice Boltzmann method, Int. J. Mod. Phys. C 24 (2013) 1350060.
[13] M. Nazari, R. Mohebbi, M. Kayhani, Power-law fluid flow and heat transfer in a channel with a built-in porous square cylinder: lattice Boltzmann simulation, J. Non-Newtonian Fluid Mech. 204 (2014) 38–49.
[14] R. Mohebbi, H. Heidari, Lattice Boltzmann simulation of fluid flow and heat transfer in a parallel-plate channel with transverse rectangular cavities, Int. J. Mod. Phys. C 28 (2017) 1750042.
[15] G.A. Bird, Molecular gas dynamics, NASA STI/Recon Technical Report A, 1976, p. 76.
[16] E. Oran, C. Oh, B. Cybyk, Direct simulation Monte Carlo: recent advances and applications, Annu. Rev. Fluid Mech. 30 (1998) 403–441.
[17] M. Basha, N.A.C. Sidik, Numerical predictions of laminar and turbulent forced convection: lattice Boltzmann simulations using parallel libraries, Int. J. Heat Mass Transf. 116 (2018) 715–724.
[18] M. Nazari, H. Shokri, M.H. Kayhani, Control of convective heat transfer by changing the right-angle position and the base angle of triangular storages: lattice Boltzmann simulation, J. Braz. Soc. Mech. Sci. Eng. 37 (2015) 149–161.
[19] A. Ismail, L. Jahanshaloo, A. Fazeli, Lagrangian grid LBM to predict solid particles' dynamics immersed in fluid in a cavity, J. Adv. Res. Fluid Mech. Therm. Sci. 3 (2014) 17–26.
[20] M. Basha, N.A.C. Sidik, Numerical simulation of fluid flow and heat transfer in rotating channels using parallel lattice Boltzmann method, Int. J. Heat Mass Transf. 115 (2017) 158–168.
[21] R. Mohebbi, M. Nazari, M. Kayhani, Comparative study of forced convection of a power-law fluid in a channel with a built-in square cylinder, J. Appl. Mech. Tech. Phys. 57 (2016) 55–68.
[22] T.J. Young, K. Vafai, Convective cooling of a heated obstacle in a channel, Int. J. Heat Mass Transf. 41 (1998) 3131–3148.
[23] P. Chandra, C. Alexander, J. Han, Heat transfer and friction behaviors in rectangular channels with varying number of ribbed walls, Int. J. Heat Mass Transf. 46 (2003) 481–495.
[24] M. Nakajima, H. Yanaoka, H. Yoshikawa, T. Ota, Numerical simulation of three-dimensional separated flow and heat transfer around staggered surface-mounted rectangular blocks in a channel, Numerical Heat Transf. Part A: Appl. 47 (2005) 691–708.
[25] B. Lu, P.-X. Jiang, Experimental and numerical investigation of convection heat transfer in a rectangular channel with angled ribs, Exp. Therm. Fluid Sci. 30 (2006) 513–521.
[26] Y.-T. Yang, C.-H. Chen, Numerical simulation of turbulent fluid flow and heat transfer characteristics of heated blocks in the channel with an oscillating cylinder, Int. J. Heat Mass Transf. 51 (2008) 1603–1612.
[27] M.A. Moussaoui, M. Jami, A. Mezrhab, H. Naji, Lattice Boltzmann simulation of convective heat transfer from heated blocks in a horizontal channel, Numerical Heat Transf. Part A: Appl. 56 (2009) 422–443.
[28] A.A. Alamyane, A. Mohamad, Simulation of forced convection in a channel with extended surfaces by the lattice Boltzmann method, Comput. Math. Appl. 59 (2010) 2421–2430.
[29] M.M. Pirouz, M. Farhadi, K. Sedighi, H. Nemati, E. Fattahi, Lattice Boltzmann simulation of conjugate heat transfer in a rectangular channel with wall-mounted obstacles, Scientia Iranica 18 (2011) 213–221.
[30] N.A.C. Sidik, M. Khakbaz, L. Jahanshaloo, S. Samion, A.N. Darus, Simulation of forced convection in a channel with nanofluid by the lattice Boltzmann method, Nanoscale Res. Lett. 8 (2013) 178.
[31] M. Izadi, A. Behzadmehr, D. Jalali-Vahida, Numerical study of developing laminar forced convection of a nanofluid in an annulus, Int. J. Therm. Sci. 48 (2009) 2119–2129.
[32] P.L. Bhatnagar, E.P. Gross, M. Krook, A model for collision processes in gases. I. Small amplitude processes in charged and neutral one-component systems, Phys. Rev. 94 (1954) 511.
[33] L. Jahanshaloo, N.C. Sidik, S. Salimi, Numerical simulation of high Reynolds number flow in lid-driven cavity using multi-relaxation time lattice Boltzmann Method, J. Adv. Res. Fluid Mech. Therm. Sci. 24 (2016) 12–21.
[34] Y. Qian, D. d'Humières, P. Lallemand, Lattice BGK models for Navier-Stokes equation, EPL (Europhys. Lett.) 17 (1992) 479.
[35] R. Mohebbi, M. Rashidi, Numerical simulation of natural convection heat transfer of a nanofluid in an L-shaped enclosure with a heating obstacle, J. Taiwan Inst. Chem. Eng. 72 (2017) 70–84.
[36] L. Jahanshaloo, N.A.C. Sidik, A. Fazeli, HA MP, An overview of boundary implementation in lattice Boltzmann method for computational heat and mass transfer, Int. Commun. Heat Mass Transf. 78 (2016) 1–12.
[37] C.-C. Chang, Y.-T. Yang, T.-H. Yen, Numerical investigation into thermal mixing efficiency in Y-shaped channel using Lattice Boltzmann method and field synergy principle, Int. J. Therm. Sci. 48 (2009) 2092–2099.
[38] S. Chen, Z. Tian, Simulation of thermal micro-flow using lattice Boltzmann method with Langmuir slip model, Int. J. Heat Fluid Flow 31 (2010) 227–235.
[39] J. Wang, D. Wang, P. Lallemand, L.-S. Luo, Lattice Boltzmann simulations of thermal convective flows in two dimensions, Comput. Math. Appl. 65 (2013) 262–286.
[40] J. Wang, M. Wang, Z. Li, A lattice Boltzmann algorithm for fluid–solid conjugate heat transfer☆☆ The present work was supported by the National Natural Science Foundation of China (Grant No. 59995550-2), Int. J. Therm. Sci. 46 (2007) 228–234.
[41] V. Trisaksri, S. Wongwises, Critical review of heat transfer characteristics of nanofluids, Renew. Sustain. Energy Rev. 11 (2007) 512–523.

[42] C.S. Nor Azwadi, O.A. Alawi, Computational investigations on heat transfer enhancement using nanorefrigerants, J. Adv. Res. Des. 1 (2014) 35–41.

[43] K. Khanafer, K. Vafai, M. Lightstone, Buoyancy-driven heat transfer enhancement in a two-dimensional enclosure utilizing nanofluids, Int. J. Heat Mass Transf. 46 (2003) 3639–3653.

[44] M.N.A.W.M. Yazid, N.A.C. Sidik, W.J. Yahya, Heat and mass transfer characteristics of carbon nanotube nanofluids: a review, Renew. Sustain. Energy Rev. 80 (2017) 914–941.

[45] Q. Li, Y. Xuan, Convective heat transfer and flow characteristics of Cu-water nanofluid, Sci. China Ser. E: Technol. Sci. 45 (2002) 408–416.

[46] M. Jamil, C.S. Nor Azwadi, M.M. Yazid, Thermal performance of thermosyphon evacuated tube solar collector using TiO$_2$/water nanofluid, J. Adv. Res. Fluid Mech. Therm. Sci. 20 (2016) 12–29.

[47] H. Brinkman, The viscosity of concentrated suspensions and solutions, J. Chem. Phys. 20 (1952) 571.

[48] H.E. Patel, K. Anoop, T. Sundararajan, S.K. Das, A micro-convection model for thermal conductivity of nanofluids, in: International Heat Transfer Conference 13, Begel House Inc., 2006.

[49] Z. Guo, C. Shu, Lattice Boltzmann Method and Its Applications in Engineering, World Scientific, 2013.

[50] M. Yousaf, S. Usman, Natural convection heat transfer in a square cavity with sinusoidal roughness elements, Int. J. Heat Mass Transf. 90 (2015) 180–190.

[51] T. Inamuro, M. Yoshino, F. Ogino, A non-slip boundary condition for lattice Boltzmann simulations, Phys. Fluids 7 (1995) 2928–2930.

[52] Q. Zou, X. He, On pressure and velocity boundary conditions for the lattice Boltzmann BGK model, Phys. Fluids 9 (1997) 1591–1598.

[53] N. Janzadeh, Delavar M. Aghajani, Using lattice Boltzmann method to investigate the effects of porous media on heat transfer from solid block inside a channel, Transp. Phenomena Nano Micro Scales 1 (2013) 117–123.

[54] R. Mei, L.-S. Luo, W. Shyy, An accurate curved boundary treatment in the lattice Boltzmann method, J. Comput. Phys. 155 (1999) 307–330.

[55] A. Mohamad, Applied lattice Boltzmann method for transport phenomena, momentum, heat and mass transfer, Can. J. Chem. Eng. 85 (2007) 946.

[56] A.K. Santra, S. Sen, N. Chakraborty, Study of heat transfer due to laminar flow of copper–water nanofluid through two isothermally heated parallel plates, Int. J. Therm. Sci. 48 (2009) 391–400.

[57] H. Heidary, M. Kermani, Effect of nano-particles on forced convection in sinusoidal-wall channel, Int. Commun. Heat Mass Transf. 37 (2010) 1520–1527.

[58] K.S. Hwang, J.H. Lee, S.P. Jang, Buoyancy-driven heat transfer of water based Al2O$_3$ nanofluids in a rectangular cavity, Int. J. Heat Mass Transf. 50 (2007) 4003–4010.